PAPER

Check for updates

Silica nanocontainers with rhodamine B acylhydrazone for early fluorescent detection of steel corrosion†

Anna Mal'tanova,‡[a] Nikita Bel'ko, [ID] ‡[b] Tatsiana Kulahava,[c] Michael Samtsov[b] and Sergey Poznyak [ID] *[a]

Developing new materials for efficient fluorescent detection of metal corrosion is a highly relevant task. One challenge is that highly sensitive sensors might lose functionality after exposure to certain coating formulations. In this work, silica nanocontainers are used to encapsulate rhodamine B acylhydrazone, an efficient pH sensor. The resulting nanomaterial is then used in water-based epoxy and acrylic coatings for early-stage detection of steel corrosion. Coatings with as little as 0.01 wt% rhodamine B acylhydrazone show a marked increase in fluorescence intensity that correlates with the onset of steel corrosion. Coatings containing the dye encapsulated in silica nanocontainers demonstrate a significantly stronger response (4 times) compared to coatings containing the dye without an encapsulating agent. Furthermore, encapsulating rhodamine B acylhydrazone improves the dispersion of this hydrophobic dye in epoxy and acrylic coating formulations without requiring an organic solvent. The ability of the resulting coatings to detect corrosion by changes in fluorescence is validated by fluorescence spectroscopy and microscopy. Impedance spectroscopy investigations indicate that silica nanocontainers improve the barrier properties of the composite epoxy coatings on steel. The encapsulation of highly sensitive and hydrophobic molecules in silica nanocontainers can be an effective method for preparing smart coatings with desired characteristics.
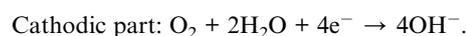
1 Introduction

Corrosion of metals is a problem of great economic importance, limiting the service life of most man-made structures and causing enormous losses. In some countries, the corrosion costs account for up to 4% of a nation's gross domestic product.[1,2] The most common method for preventing the corrosion of metallic structures is the application of organic coatings.[3,4] Although this measure can substantially delay the destruction of a metal structure, any coating has a finite life, and a complete inhibition of corrosion is unattainable. This is particularly true for metal structures exposed to aggressive environmental factors, such as seawater, humidity, high temperatures, *etc*. In such conditions, most polymeric systems fail to prevent the ingress of corrosion-aggressive ions like Cl^-. Ultimately, this leads to the onset of corrosion and the destruction of the protective oxide layer, promoting the local dissolution of metals. For this reason, smart coatings are being developed to provide active protection and early detection of corrosion of the underlying metal.

Upon the onset of corrosion in neutral media, the following set of redox reactions takes place:[5,6]

$$\text{Anodic part: } Me \rightarrow Me^{n+} + ne^-$$

$$\text{Cathodic part: } O_2 + 2H_2O + 4e^- \rightarrow 4OH^-.$$

Apart from electrochemical reactions, the acid–base interaction occurs. The metal dissolution leads to the formation of metal ions. The hydrolysis of the ions results in the formation of hydroxide complexes accompanied by acidification:[7]

$$Me \rightarrow Me^{n+} + ne^-$$

$$Me_{aq}^{n+} + H_2O \leftrightarrow (Me(OH))_{aq}^{(n-1)+} + H_{aq}^+.$$

At the same time, the hydroxide ions (OH^-) formed at the cathodic side provoke alkalization.

[a]*Research Institute for Physical Chemical Problems, Belarusian State University, Leningradskaya Str. 14, 220006 Minsk, Belarus. E-mail: poznyak@bsu.by*

[b]*A. N. Sevchenko Institute of Applied Physical Problems, Belarusian State University, Kurchatova Str. 7, 220045 Minsk, Belarus*

[c]*Institute for Nuclear Problems, Belarusian State University, Bobruiskaya Str. 11, 220006, Minsk, Belarus*

† Electronic supplementary information (ESI) available: Photographs of SiNCs and free-standing epoxy films; cross-sectional SEM images of epoxy and acrylic coatings on steel; nitrogen adsorption isotherm, XRD pattern, TG/DSC curves, and FTIR spectrum for SiNCs; absorption spectra for RBA@SiNCs in aqueous suspension. See DOI: https://doi.org/10.1039/d4ra07677j

‡ These authors contributed equally to this work.

Early detection of corrosion can be achieved by applying organic coatings that contain fluorescent dyes capable of sensing metal ions or changes in pH.[8–14] However, preparing such coatings presents a challenge as the incorporated dyes must be sensitive to the corrosion process while maintaining their structure and spectral properties when introduced into a coating formulation. Coating formulations may exhibit high acidity or alkalinity and contain reactive components, which may result in a loss of functionality of pH-sensitive sensors. To prevent this, sensors can be encapsulated in inert nano-containers before being added to a coating formulation.

Several types of encapsulation agents were previously reported in the literature. Layered double hydroxides,[15,16] clays,[11,17] and polymeric nano- and microcapsules[11,18] have been used in smart coatings for corrosion detection and prevention. Silica nanocontainers (SiNCs) are excellent candidates for encapsulating various active compounds due to their mild and facile one-step synthesis process and high loading capacity.[19,20] SiNCs have been successfully utilized to prepare smart coatings loaded with corrosion inhibitors,[20] sensors,[21] or biocides.[22] The encapsulation in SiNCs can prevent interactions between active compounds and the coating, while ensuring a controlled release of the contents of the containers.

Rhodamine B acylhydrazone (RBA) has been used as an indicator in smart epoxy coatings to detect steel corrosion in early stages due to its high sensitivity toward ferric ions.[9] However, as shown in our previous work, the dye is susceptible to hydrolysis under acidic pH.[23] This finding suggests that the dye may lose its functionality when exposed to certain coating formulations. Furthermore, RBA is a water-insoluble compound and cannot be directly added to water-based coating formulations. More recently, Wang et al. successfully demonstrated the use of ~5 μm large silica structures as a support for RBA in the preparation of smart coatings for early corrosion detection.[24]

In contrast to the mentioned study, we employ the microemulsion method,[20] which results in the formation of spherical, 100 nm large SiNCs. In this work, SiNCs are utilized for the encapsulation of RBA due to several key reasons: (1) SiNCs prevent the transformation of this pH-sensitive dye when introduced into coating formulations; (2) RBA-loaded SiNCs are readily integrated into water-based coatings without the need for an organic phase; (3) SiNCs guarantee optimal dispersion of the dye within a coating, which is particularly important for eco-friendly, water-based formulations; (4) RBA remains entrapped in SiNCs while its fluorescence is activated under service conditions. The properties of epoxy and acrylic coatings containing RBA-loaded SiNCs are studied using fluorescence spectroscopy and microscopy along with electrochemical impedance spectroscopy. Coatings containing RBA-loaded SiNCs and coatings with directly added RBA are compared.

2 Experimental

2.1 Materials

RBA (3′,6′-bis(diethylamino)-2-(propan-2-ylideneamino)spiro [isoindole-3,9′-xanthene]-1-one) was synthesized following the procedure described in ref. 23. Toluene (anhydrous, 99.8%),

dichloromethane (>99.8%), MeCN (>99.9%), EtOH (>95%), 25% aqueous ammonia solution, $FeCl_3 \cdot 6H_2O$ (97%), NaCl (99%), and 37% HCl were purchased from Sigma-Aldrich. Cetyl-trimethylammonium bromide (CTAB, >99%) and tetraethoxysilane (TEOS, 98%) were purchased from Acros Organics.

Epoxy coatings were prepared using the water-based CHS-Epoxy 200 V 55 (Spolchemie) epoxy resin with the Telalit 180 (Spolchemie) hardener (w/w = 100 : 27). Acrylic coatings were prepared using a water-based acrylic emulsion 76 (Bisley International LLC).

2.2 Synthesis of SiNCs

Bare SiNCs were prepared via the single-step polymerization process in an oil-in-water microemulsion, as described in ref. 20, with some modifications. TEOS served as a precursor of silica, CTAB was used as a cationic surfactant, and 25% ammonia solution was used as a catalyst. Toluene or dichloromethane was used as a co-solvent. Initially, 0.1 g CTAB was dissolved in 35 mL deionized (DI) water. After allowing the surfactant to swell for 2 h, 0.25 mL ammonia solution was added. Then, 25 mL co-solvent was added dropwise under vigorous stirring to form a microemulsion. Next, 2 mL TEOS was added, and the emulsion was kept under vigorous stirring for the following 24 h. Finally, the precipitate was filtered using a paper filter (PRAT DUMAS) with a pore size of 2–3 μm, washed with DI water, and dried at 40 °C for 24 h.

To prepare SiNCs loaded with RBA (RBA@SiNCs), 50 mg of the dye was dissolved in 25 mL of a co-solvent before adding it to the aqueous phase. When dichloromethane was used as the co-solvent, the emulsion gradually turned from white to light pink. RBA was previously shown to undergo protonation and spirolactam ring opening under acidic pH, resulting in pink color.[23] The color change in the emulsion may be attributed to the oxidation of dichloromethane in air, resulting in the formation of HCl, a decrease in pH, and the subsequent protonation of RBA. When toluene was used as the co-solvent, the microemulsion remained white during the synthesis. However, after the precipitate was filtered, it acquired a pinkish hue, which may be due to a slight decrease in pH associated with the hydrolysis of silica. The color of RBA@SiNCs prepared using toluene as the co-solvent was barely visible, while RBA@SiNCs prepared using dichloromethane had a much more pronounced pinkish hue (Fig. S1†). The following studies focus on SiNCs and RBA@SiNCs that were prepared using toluene as the co-solvent. The oxidation of chlorinated organic solvents should be considered when preparing SiNCs loaded with pH-sensitive molecules.

To determine RBA content in SiNCs, 1 mg RBA@SiNCs was dispersed in 1 mL MeCN and sonicated for 2 h. The suspension was then centrifuged at 12 000 rpm for 10 min, and the concentration of RBA in the supernatant was determined using spectrophotometry. The dye content in SiNCs was found to be 1.6 wt%.

2.3 Preparation of coatings

Either RBA@SiNCs (0.5 wt%) or an equivalent amount of pure RBA (7.2×10^{-3} wt%) was added to coating formulations. To

ensure the dispersion of RBA@SiNCs in coating formulations, the nanomaterial was first dispersed in DI water at a concentration of 4.5 mg mL^{-1} and sonicated for 15 min. The resulting suspension was centrifuged at 12 000 rpm for 10 min, and the supernatant was decanted. The remaining slurry was then thoroughly mixed with coating formulations. Pure RBA was dissolved in EtOH and added to coating formulations at 5 wt% EtOH.

For epoxy coatings, the epoxy resin was mixed with RBA@SiNCs (as wet slurry) or pure RBA (as EtOH solution) followed by the addition of the hardener. Free-standing (not attached to a substrate) epoxy films were prepared by pouring the epoxy coating formulation into a silicone mold and curing it for 72 h at room temperature. The resulting films were 1.1 mm thick. For acrylic coatings, RBA@SiNCs (as wet slurry) or pure RBA (as EtOH solution) were mixed with the water-based acrylic emulsion. Free-standing acrylic films were not prepared.

Samples for corrosion sensing were prepared on A622DQ carbon steel coupons measuring $5.0 \times 3.0 \times 0.1$ cm. The steel contained C (0.08 wt%), Mn ($\leq$0.40 wt%), P ($\leq$0.03 wt%), and S ($\leq$0.03 wt%). This type of metal was chosen for the measurements in the described model system because low-carbon steels are prone to corrosion in the presence of chloride ions.[25,26] The steel coupons were sandblasted and degreased with EtOH. Coating formulations containing RBA@SiNCs or pure RBA were applied to one side of the coupons. These formulations were tape-cast onto the coupons using a casting blade and left to cure for 72 h at room temperature. The thickness of cured epoxy and acrylic coatings, as measured using scanning electron microscopy (SEM), was 50 and 18 μm, respectively (Fig. S2†). The back and edges of the steel coupons were brush-coated with the corresponding blank formulations.

2.4 Characterization

The morphology of the synthesized SiNCs and RBA@SiNCs was characterized using a Hitachi S-4800 scanning electron microscope at an operating voltage of 15 kV in the secondary electron detection mode. Particle size distribution was then determined using the ImageJ software.

The specific surface area and porous structure of SiNCs were estimated by nitrogen adsorption at 77 K and a gradual increase in pressure using a QuadraSorb SI device. The specific surface area was calculated using the Brunauer–Emmett–Teller (BET) theory. The pore sizes were determined using the Barrett–Joyner–Halenda (BJH) model. Before the measurements, the samples were degassed by heating in a helium stream at a temperature of 250 °C for 2 h. Thermogravimetry/differential scanning calorimetry (TG/DSC) measurements were carried out using a NETZSCH STA 449C thermal analyzer in the 20–800 °C temperature range in air at a heating rate of 10 °C min^{-1}. X-ray diffractometry (XRD) measurements were performed on a PANalytical Empyrean diffractometer using CuKα-radiation. The recording speed was 0.4° min^{-1}. Fourier-transform infrared (FTIR) spectrum was collected using a PerkinElmer Spectrum Two FT-IR spectrometer.

The optical properties of the prepared coatings were characterized using fluorescence spectroscopy and microscopy.

Fluorescence spectra were acquired for RBA@SiNCs suspensions, free-standing epoxy films, and coated steel coupons using a Horiba Scientific Fluorolog 3 spectrofluorimeter. RBA@SiNCs suspensions were placed in 1 mm quartz cuvettes, and their fluorescence spectra were measured in the front-face geometry. Absorption spectra for aqueous suspensions of RBA@SiNCs were measured using a SOLAR PV1251 spectrophotometer in 1 cm quartz cuvettes. The coated steel samples were immersed in 0.5 M aqueous NaCl solution to accelerate steel corrosion. Fluorescence microscopy images were captured using an inverted Nikon Eclipse Ti2 microscope with a 10× Nikon CFI Plan Fluor DLL objective (0.3 NA). The excitation light source was an LED with an emission peak at 554 nm and a FWHM of 23 nm. The emission signal was filtered using a BrightLine Pinkel filter set (576–615 nm emission band) and detected with a TOUPTEK ToupCam E3ISPM09000KPB color camera equipped with a 9 MP color CMOS matrix sensitive in the 380–650 nm range.

The corrosion process in a chloride-containing solution was monitored *in situ* using electrochemical impedance spectroscopy (EIS). EIS measurements were conducted at room temperature using a three-electrode cell with an Ag/AgCl/KCl (sat.) reference electrode, a 3 cm^2 Pt foil as a counter electrode, and the coated steel samples serving as a working electrode. Acrylic glass tubes (2.5 cm in diameter, 5 cm high) were glued to the surface of coated steel samples and filled with 0.5 M aqueous NaCl solution. Long-term corrosion testing was periodically performed by impedance measurements. The NaCl solution initiated the corrosion process and served as the supporting electrolyte for the EIS measurements. During the measurements, the electrochemical cell was placed in a Faraday cage to prevent interference from external electromagnetic fields. Impedance was measured in the range of 100 kHz to 0.1 Hz using a Metrohm Autolab PGSTAT 302N potentiostat/galvanostat. All impedance spectra were acquired at the open-circuit potential, with 10 mV sinusoidal perturbations. Before acquiring the spectra, the system was allowed to reach a stable open circuit potential.

3 Results and discussion

As shown in Fig. 1, the SiNCs and RBA@SiNCs synthesized with toluene as the co-solvent had a uniform spherical shape with mean diameters of 110 ± 8 and 126 ± 9 nm, respectively (averaged over 200 particles). Encapsulation of RBA slightly increased the dimensions of SiNCs without compromising their shape. SiNCs exhibited a type IV isotherm with a N$_2$ hysteresis loop at a relative pressure (P/P_0) of 0.4–1.0 (Fig. S3†), which is characteristic of mesoporous solids.[27] The specific surface area of SiNCs was 488.9 m^2 g^{-1}, and the average pore diameter was 3.6 nm. The XRD pattern (Fig. S4†) indicates that the prepared SiNCs possessed amorphous structure.[20]

TG/DSC analysis was performed to examine thermal properties of the prepared SiNCs. The low-temperature endothermic events in the DSC curve (peaking at 76 and 248 °C) were accompanied by a *ca.* 4% mass loss (Fig. S5†). These effects probably reflected the removal of weakly bound water molecules
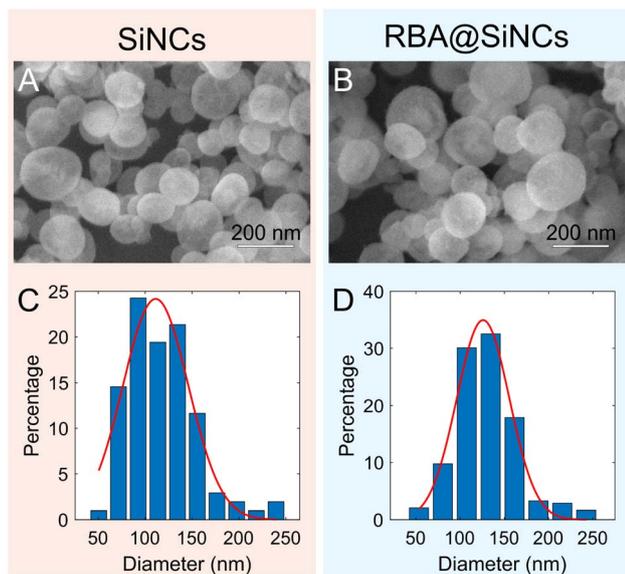
Fig. 1 SEM images (A and B) and histograms of the size distribution (C and D) for SiNCs (A and C) and RBA@SiNCs (B and D).

from the mesopores in SiO_2.[28] At temperatures above 250 °C, an exothermic event was evident (peaking at 339 °C), coupled to a substantial mass loss of *ca.* 22%. This exothermic event could be due to the oxidation of organic compounds (in particular, CTAB and non-polymerized TEOS) that were used during the synthesis of SiNCs and remained adsorbed on their surface.[20,28] The mass loss in the 400–800 °C range was *ca.* 5% and could be linked to the removal of chemically bound hydroxyl groups.[29] The exothermic event occurring at temperatures above 800 °C was probably connected to the onset of SiO_2 crystallization.[30]

FTIR spectrum for SiNCs exhibited bands characteristic of amorphous hydroxylated silica peaked at 1066, 964, 797, 565, and 451 cm^{-1} (Fig. S6†). The bands at 1066 and 797 cm^{-1} correspond to the stretching vibrations of the Si–O–Si and Si–O bonds, and the bands at 964 and 451 cm^{-1} belong to the deformation vibrations of the Si–OH and Si–O–Si bonds.[31] The band at 565 cm^{-1} can be assigned to Si–O–Si bending vibrations of the tetrahedra of silicate groups. The observed frequencies of the deformation vibrations of the Si–O–Si bonds are characterized by lower values compared to crystalline silica due to the presence of water in the xerogel structure. This is confirmed by the presence of bands at 1642 and ∼3350 cm^{-1}, which correspond to the bending vibrations of H_2O and the asymmetric stretching vibrations of –OH groups in the prepared sample, respectively.[32]

The corrosion process is associated with a local decrease in pH and an increased concentration of Fe^{3+} ions.[5] Colorimetric and fluorescent responses of RBA to these stimuli were studied in solution in our previous work.[23] A substantial increase in absorbance and fluorescence intensity in the visible range is detected immediately when 25 μM H$^+$ or Fe^{3+} ions is added to a 25 μM solution of RBA. These effects are the result of the protonation of RBA accompanied by the opening of the spirolactam ring. Then, the absorbance and fluorescence gradually

decay (over several hours) due to the hydrolysis of RBA, which leads to the formation of rhodamine B hydrazide. Both the protonation and the hydrolysis of RBA are acid-catalyzed. As a result, the dye cannot sense Fe^{3+} ions directly. Rather, the response of RBA is triggered by the drop in pH caused by the hydrolysis of Fe^{3+} ions. At higher concentrations of RBA and added ions, the amount of protonated dye molecules and the rate of hydrolysis increase. For instance, at 1.3 mM RBA and 13.0 mM added H$^+$ or Fe^{3+} ions, RBA is fully hydrolyzed in 20 min.

The nanoencapsulation of RBA in SiNCs was performed in an attempt to inhibit the hydrolysis of RBA thus enabling a stable response for long-term monitoring. The colorimetric and fluorescent responses of RBA@SiNCs to corrosion-related stimuli (namely, added H$^+$ or Fe^{3+} ions) were first investigated in suspensions. An aqueous suspension of as-prepared RBA@SiNCs showed weak fluorescence under 510 nm excitation. After exposure to 5 mM H$^+$ (as HCl) or Fe^{3+} (as FeCl$_3$) for 1 month, the fluorescence intensity increased 3- and 10-fold, respectively (Fig. 2). The absorbance of RBA@SiNCs exposed to 5 mM H$^+$ ions steadily increased over the course of 22 days (Fig. S7a†), while the absorbance of RBA in solution was shown to decrease due to hydrolysis.[23] The release of RBA from SiNCs was also studied. RBA@SiNCs were exposed to 5 mM aqueous HCl for 22 days, and then the supernatant of the suspension was collected. The absorbance of the dye in the supernatant turned out to be 10 times lower compared to the suspension (Fig S7b†). We can conclude that the colorimetric and fluorescent responses mostly stem from the dye encapsulated in SiNCs, and the release of RBA into the supernatant is almost negligible. The hydrolysis of dye molecules entrapped in SiNCs seems to be inhibited.

The fluorescence response of RBA@SiNCs was also tested in free-standing epoxy films. Epoxy films with RBA@SiNCs or with directly added RBA were immersed in 0.1 M aqueous solutions
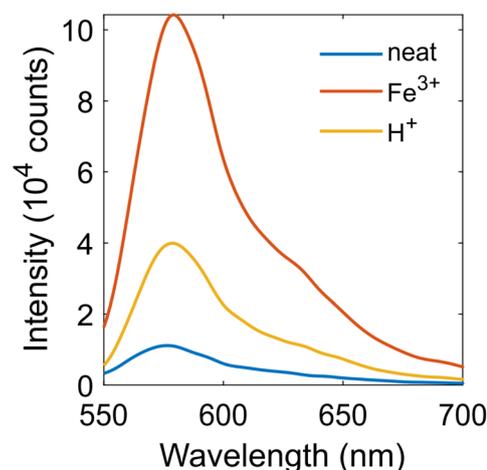

Fig. 2 Fluorescence spectra excited at 510 nm for 1 mg mL^{-1} aqueous suspensions of RBA@SiNCs: as prepared (blue curve) and after a 1 month exposure to 5 mM Fe^{3+} (red curve) or H$^+$ (yellow curve). As Fe^{3+} ions exhibit strong light absorption in the visible range, they were removed by washing RBA@SiNCs with centrifugation before acquiring the spectrum.
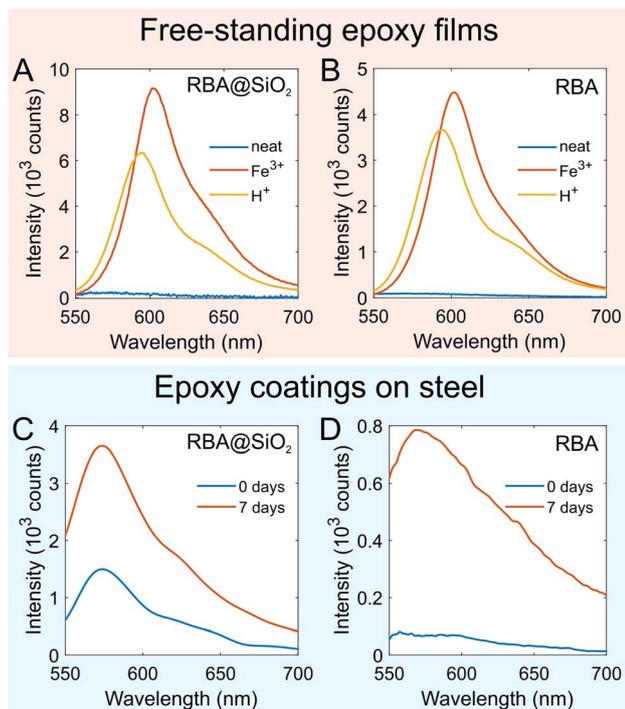
Fig. 3 (A and B) Fluorescence spectra excited at 510 nm for free-standing epoxy films with RBA@SiNCs (A) and with directly added RBA (B): as prepared (blue curves) and after 2 months of exposure to 0.1 M aqueous Fe^{3+} (red curves) or H^+ (yellow curves). (C and D) Fluorescence spectra excited at 510 nm for epoxy coatings on steel with RBA@SiNCs (C) and with directly added RBA (D): as prepared (blue curves) and after 7 days of exposure to 0.5 M aqueous NaCl (red curves).

of $FeCl_3$ or HCl. No color changes or fluorescence were observed over a 3 days period. However, after 10 days, weak fluorescence appeared, whereas the as-prepared films were virtually non-fluorescent. After 2 months of exposure to Fe^{3+} or H^+, the epoxy films showed intense fluorescence under 510 nm excitation (Fig. 3A and B). The peak of the spectra for the epoxy films exposed to Fe^{3+} was red-shifted by 8 nm, which could be due to light absorption by Fe^{3+} ions adsorbed on the films. Since the diffusion of H^+ and Fe^{3+} ions through the epoxy resin was rather slow, the strong fluorescent response was observed only after a long period of time, which is not always practical. However, the free-standing epoxy films were over 1 mm thick, which greatly exceeds the typical thickness of coatings applied on metals. Remarkably, the change in color of an epoxy film filled with RBA@SiNCs could even be observed with the naked eye (Fig. S8†).

RBA@SiNCs developed fluorescent and colorimetric responses to H^+ or Fe^{3+} ions substantially slower compared to free RBA molecules in solution. The incorporation of RBA@SiNCs into an epoxy matrix further retarded these processes. On one hand, this can be considered as reduced sensitivity of RBA inside such a composite system. On the other hand, the drastic reduction in the hydrolysis rate allow us to avoid the drop in fluorescence intensity over time observed for RBA in solution. To trigger a response of RBA@SiNCs inside an epoxy matrix, the

external stimuli should be strong and prolonged, thus protecting this system from false sensitivity.

More importantly, coatings should exhibit a response to the corrosion of the underlying metal. To that end, the performance of RBA@SiNCs was studied in an epoxy coating applied on a steel coupon. The coating was scribed to accelerate the corrosion process. As mentioned in Section 2.2, RBA@SiNCs had a pinkish hue, possibly due to silica hydrolysis. Consequently, the as-prepared epoxy coating with RBA@SiNCs showed weak fluorescence under 510 nm excitation. After being immersed in 0.5 M NaCl solution for 7 days, the fluorescence signal increased 3-fold (Fig. 3C). It should be noted that the fluorescence signal was collected from an area of ~5 mm^2, while the most pronounced response of the coating was expected in the vicinity of the scribed area. As a result, the actual response of the coating was significantly stronger than what was reflected in the fluorescence spectra. To illustrate this point, the changes in fluorescence were also imaged using fluorescence microscopy (Fig. 4A). The onset of corrosion was clearly visualized by the fluorescence of RBA@SiNCs just after 1 day of immersion in NaCl solution.
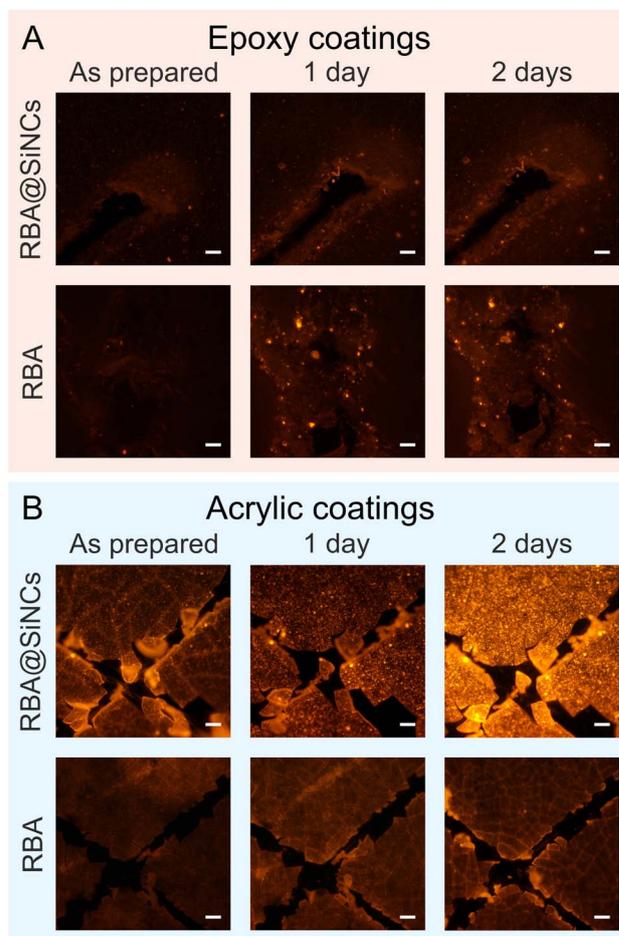

Fig. 4 Fluorescence microscopy images for scribed epoxy (A) and acrylic (B) coatings on steel with RBA@SiNCs and with directly added RBA: as prepared and after 1 day and 2 days of exposure to 0.5 M aqueous NaCl. The bars are equal to 100 μm.

The performance of an epoxy coating with directly added RBA was also examined. After immersion in 0.5 M NaCl for 7 days, the coating showed a significant increase in fluorescence intensity (Fig. 3D and 4A). However, the resulting intensity was *ca.* 4 times lower compared to the coating containing RBA@-SiNCs with the same dye content. This difference could be attributed to the degradation of the dye exposed to epoxy resin and hardener and/or the crystallization and poor dispersion of RBA in the coating formulation. Thus, the encapsulation of RBA in SiNCs led to a stronger fluorescence response while eliminating the need for organic solvents in coating formulations. This resulted in increased efficiency of corrosion detection and allowed for the use of coatings with a low dye content (<0.01 wt%), leading to a lower price. In a previous work,[9] a substantially larger amount of RBA (0.5 wt%) was directly added to epoxy coatings for the detection of steel corrosion.

EIS measurements were performed to gain additional information on the anticorrosion efficiency of the prepared coatings. The Bode plots (Fig. 5A) indicate that epoxy coatings

with RBA@SiNCs and directly added RBA initially have similar values of the impedance modulus ($|Z|$). After 7 days of exposure to 0.5 M aqueous NaCl, the impedance drops for both coatings, but $|Z|$ at low frequencies ($f = 0.1$ Hz) is 6 times higher for the coating with RBA@SiNCs compared to the coating with directly added RBA. As $|Z|$ at low frequencies correlates in a certain way with the corrosion resistance, the evolution of $|Z|$ is illustrated in Fig. 5B. These data indicate that SiNCs improve the barrier properties of epoxy coatings thus delaying their failure.

Despite the durability and prevalence of epoxy coatings, some applications may require other types of coating formulations, such as acrylic emulsions, which do not require a hardener. An acrylic coating with RBA@SiNCs shows a strong local increase in fluorescence intensity caused by the onset of corrosion (Fig. 4B). In contrast, an acrylic coating with directly added RBA exhibits a very weak response to the corrosion process, which could be due to the degradation or crystallization of the dye in the water-based acrylic emulsion.

4 Conclusions

Epoxy and acrylic coatings containing RBA@SiNCs and directly added RBA were prepared and tested for their ability to detect the onset of steel corrosion. The results showed that the epoxy coatings with both RBA@SiNCs and directly added RBA were effective in visualizing corrosion. The fluorescence response of the coating with RBA@SiNCs was three times higher than that of the coating with directly added RBA. The acrylic coating containing RBA@SiNCs also showed a strong response to the corrosion process, while the coating with directly added RBA was significantly less effective. EIS measurements revealed that the presence of SiNCs in epoxy coatings improved their barrier properties.

Encapsulating RBA in SiNCs enabled the preparation of coatings with well-dispersed dye without the need for organic solvents. The coatings demonstrated a marked response to the onset of corrosion despite the low dye content (<0.01 wt%).

This work was meant to describe an approach to the preparation of smart coatings containing a sensitive pH sensor. SiNCs were shown to be an effective carrier for incorporating hydrophobic and sensitive organic compounds into various coating formulations, including water-based and eco-friendly ones. At this point, the method is not fully optimized and was tested on a rather small set of coating formulations. Low-carbon steel was chosen to accelerate the corrosion process. The corrosion medium contained 0.5 M Cl^- ions, representing a rather aggressive environment. In industrial applications, conditions would be different, calling for further optimization of the described method. In addition, future work will concentrate on the search for other organic compounds that could be encapsulated in SiNCs and used in smart coatings.

Fig. 5 EIS measurements performed for epoxy coatings on steel with RBA@SiNCs and directly added RBA to follow the corrosion process. (A) Bode plots measured after 0.2 and 168 h of exposure to 0.5 M aqueous NaCl. (B) Impedance modulus ($|Z|$) at a frequency $f = 0.1$ Hz as a function of exposure time to 0.5 M aqueous NaCl.

Data availability

The data supporting this article have been included as part of the manuscript and its ESI.† The original files will be made available on request.
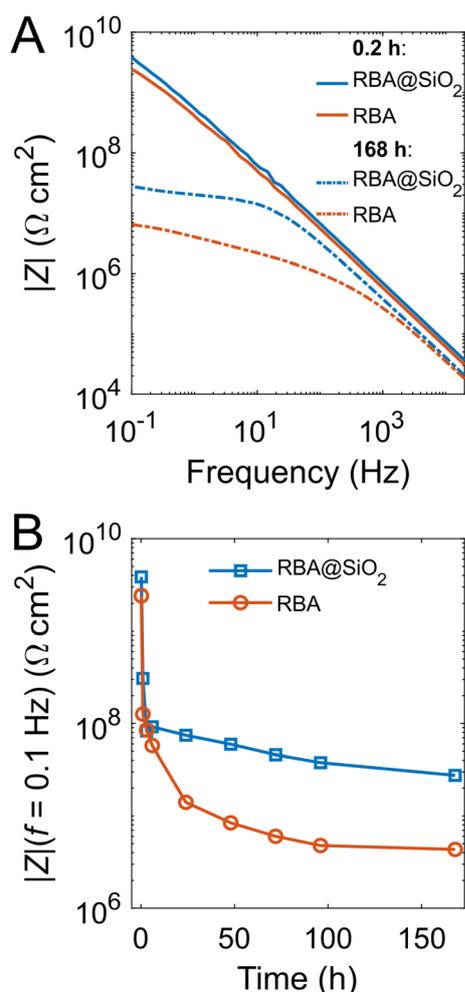
Author contributions

Anna Mal'tanova: data curation, investigation, methodology, writing – original draft. Nikita Bel'ko: data curation, investigation, methodology, visualization, writing – original draft. Tatsiana Kulahava: data curation, investigation, methodology, visualization, writing – review & editing. Michael Samtsov: conceptualization, methodology, supervision, writing – review & editing. Sergey Poznyak: conceptualization, investigation, methodology, supervision, writing – review & editing.

Conflicts of interest

There are no conflicts to declare.

Acknowledgements

Notes and references

1 D. M. Bastidas, *Metals*, 2020, **10**, 458.
2 G. Koch, *Trends in Oil and Gas Corrosion Research and Technologies*, Woodhead Publishing, Boston, 2017, pp. 3–30.
3 S. B. Lyon, R. Bingham and D. J. Mills, *Prog. Org. Coat.*, 2017, **102**, 2–7.
4 G. P. Bierwagen, *Prog. Org. Coat.*, 1996, **28**, 43–48.
5 J. R. Galvele, *J. Electrochem. Soc.*, 1976, **123**, 464.
6 N. A. North and I. D. MacLeod, *Conservation of Marine Archaeological Objects*, Elsevier, 1987, pp. 68–98.
7 G. Frankel, *J. Electrochem. Soc.*, 1998, **145**, 2186.
8 D. Bryant and D. Greenfield, *Prog. Org. Coat.*, 2006, **57**, 416–420.
9 A. Augustyniak, J. Tsavalas and W. Ming, *ACS Appl. Mater. Interfaces*, 2009, **1**, 2618–2623.
10 A. Augustyniak and W. Ming, *Prog. Org. Coat.*, 2011, **71**, 406–412.
11 I. Cole, *Handbook of Smart Coatings for Materials Protection*, Woodhead Publishing, 2014, pp. 29–55.
12 G. Dhole, G. Gunasekaran, T. Ghorpade and M. Vinjamur, *Prog. Org. Coat.*, 2017, **110**, 140–149.
13 S. Roshan, A. A. S. Dariani and J. Mokhtari, *Appl. Surf. Sci.*, 2018, **440**, 880–888.
14 D. A. Braasch, M. Gillis, M. Pramanik, R. C. Ferguson, D. Delatte, M. Blanton and J. W. Rawlins, *ACS Appl. Mater. Interfaces*, 2019, **11**, 37193–37208.
15 J. Lv, Q.-x. Yue, R. Ding, W.-h. Li, X. Wang, T.-j. Gui and X.-d. Zhao, *J. Taiwan Inst. Chem. Eng.*, 2021, **118**, 309–324.
16 M. J. Anjum, J. Zhao, V. Z. Asl, G. Yasin, W. Wang, S. Wei, Z. Zhao and W. Q. Khan, *Corros. Sci.*, 2019, **157**, 1–10.
17 T. Mishra, A. Mohanty and S. Tiwari, *Key Eng. Mater.*, 2013, **571**, 93–109.
18 A. C. M. Silva, A. D. Moghadam, P. Singh and P. K. Rohatgi, *J. Coat. Technol. Res.*, 2017, 1–29.
19 H. Chen, J. He, H. Tang and C. Yan, *Chem. Mater.*, 2008, **20**, 5894–5900.
20 F. Maia, J. Tedim, A. D. Lisenkov, A. N. Salak, M. L. Zheludkevich and M. G. Ferreira, *Nanoscale*, 2012, **4**, 1287–1298.
21 D. Mata, N. Scharnagl, S. Lamaka, E. Malheiro, F. Maia and M. Zheludkevich, *Corros. Sci.*, 2018, **140**, 307–320.
22 F. Maia, A. Silva, S. Fernandes, A. Cunha, A. Almeida, J. Tedim, M. Zheludkevich and M. Ferreira, *Chem. Eng. J.*, 2015, **270**, 150–157.
23 N. Belko, H. Maltanava, A. Lugovski, R. A. Ferreira, S. F. Correia, P. Shabunya, S. Fatykhava, A. Tabolich, T. Kulahava, A. Bahdanava, *et al.*, *Microchem. J.*, 2023, **191**, 108744.
24 Q. Wang, Y. Song, Y. Liu, J. Wang, C. Huang, Z. Xie and B. Liu, *J. Electroanal. Chem.*, 2024, **972**, 118641.
25 G. Qi, X. Qin, J. Xie, P. Han and B. He, *RSC Adv.*, 2022, **12**, 20929–20945.
26 S. O. Alharbi, S. Ahmad, T. Gul, I. Ali and A. Bariq, *Sci. Rep.*, 2024, **14**, 5098.
27 K. S. W. Sing, *Pure Appl. Chem.*, 1985, **57**, 603–619.
28 Y. Song, F. Zhao, Z. Li, Z. Cheng, H. Huang and M. Yang, *RSC Adv.*, 2021, **11**, 23901–23907.
29 A. Blinov, A. Blinova, A. Kravtsov, A. Gvozdenko, A. Kobina and E. Momot, *AIP Conf. Proc.*, 2019, **2188**, 040011.
30 M. Borouni, B. Niroumand and A. Maleki, *J. Solid State Chem.*, 2018, **263**, 208–215.
31 A. Murashkevich, A. Lavitskaya, T. Barannikova and I. Zharskii, *J. Appl. Spectrosc.*, 2008, **75**, 730–734.
32 B. Shi, L. Xie, B. Ma, Z. Zhou, B. Xu and L. Qu, *Gels*, 2022, **8**, 744.